Thermoluminescence dose response and kinetic parameters of Gd-doped ZnO nanoparticles

M. Isik[a,*], T. Yildirim[b], M. Guner[c], N.M. Gasanly[d,e]

[a]*Department of Electrical and Electronics Engineering, Atilim University, 06836 Ankara, Türkiye*
[b]*Department of Physics, Aksaray University, 68100 Aksaray, Türkiye*
[c]*Department of Physics, Nevşehir Haci Bektaş Veli University, 50300 Nevşehir, Turkey*
[d]*Department of Physics, Middle East Technical University, 06800 Ankara, Türkiye*
[e]*Virtual International Scientific Research Centre, Baku State University, 1148 Baku, Azerbaijan*

Abstract

This study investigates the thermoluminescence (TL) properties of undoped and gadolinium (Gd)-doped zinc oxide (ZnO) nanoparticles synthesized via sol-gel method. The crystal structure of both synthesized nanoparticles was determined as hexagonal from x-ray diffraction pattern. The TL curve of undoped ZnO nanoparticles reveals two distinct peaks at 400.5 and 479.2 K, each associated with trap centers featuring activation energies of 0.84 and 1.05 eV. TL curve of the Gd:ZnO introduced three peaks associated with trap centers at 1.10, 1.18, and 1.25 eV. Notably, the absence of the 0.84 eV trap center in Gd-doped ZnO implies a modification in the defect structure. Considering the effect of Gd-doping on the band structure and potential minor errors in the analysis results, it was stated that the traps at 1.05 and 1.10 eV levels belonged to the same defect center. Dose-dependent investigations for undoped and Gd-doped ZnO nanoparticles reveal linear behaviors in the TL response, highlighting their potential for dosimetric applications. Photoluminescence spectra of both compounds exhibited emission peaks around 455 and 577 nm, which were associated with native defect centers.

Keywords: ZnO, thermoluminescence, dosimetry, dose dependence, doping, defects

Published by PHYSICA SCRIPTA
https://doi.org/10.1088/1402-4896/ad52fa

1. Introduction

Zinc oxide (ZnO) stands out as a highly promising material with multifaceted applications in microelectronics and optoelectronics [1–3]. The material's alluring combination of optical and electrical properties has positioned it at the forefront of technological advancements, finding utility in an array of applications ranging from solid-state emission and electroluminescent devices [4] to piezoelectric transducers [5], transparent electrodes [6], photo-catalysts [7], chemical sensors [8], and solar cells [9]. Despite its well-established prowess in these diverse domains, ZnO has, until recently, encountered a lack of consideration as a dosimetric material. This relative neglect may be attributed to the material's prominent roles in optoelectronics and the historically reported low thermoluminescence (TL) emission efficiency in prior studies on ZnO samples [10,11]. The luminescent characteristics of ZnO are linked to its electronic and crystalline structure, factors profoundly influenced by both the preparation method and the incorporation of dopants. As the scientific community delves deeper into understanding the dosimetric potential of materials, ZnO's underexplored capacity is gaining attention. Exploring ZnO's dosimetric properties entails a comprehensive analysis, tapping into the impact of dopants, thereby unraveling new possibilities for radiation sensing and measurement technologies. In this context, it becomes imperative to bridge the gap between the established functionalities of ZnO in optoelectronic applications and its emergent role as a dosimetric material.

The impact of defects on the performance of optoelectronic devices stands as a well-explored domain within the scientific discourse. In optoelectronic devices such as light-emitting diodes (LEDs) or lasers, defects play a critical role by introducing nonradiative recombination centers [12,13]. These centers have the potential to impede light generation altogether, contingent upon the defect density. In electronic devices, defects act as scattering centers, diminishing carrier mobility and impeding the devices' high-frequency operation. Consequently, the precise characterization of defect center parameters is important in both fundamental research and technical applications.

Among the methodologies employed for determining these crucial defect parameters, thermoluminescence (TL) emerges as a particularly pertinent approach [14]. This technique based on the analysis of the temperature dependence of the emitted photon count, resulting from the recombination of excited charge carriers from trap centers with their opposite charge carriers in the recombination centers. The strategic application of TL provides invaluable insights into the nature and characteristics of defects within the material, facilitating

a detailed understanding of their influence on optoelectronic device performance. Researchers have conducted several studies exploring the photoluminescence, thermoluminescence, and dosimetric characteristics of undoped and doped ZnO materials [15–18]. However, a notable gap exists in the literature regarding the thermoluminescence and dosimetric properties of gadolinium (Gd)-doped ZnO nanoparticles synthesized through the nitric acid method. The absence of reported findings in this domain prompted our investigation, revealing the TL and dosimetric attributes exhibited by undoped and Gd-doped ZnO nanoparticles when subjected to beta irradiation. This contribution not only expands the current understanding of ZnO nanoparticle's behavior under irradiation but also introduces valuable insights into the potential enhancements introduced by Gd doping, setting the stage for further exploration in radiation dosimetry.

2. Experimental details

Zinc oxide (ZnO) nanocrystals were synthesized via the sol-gel method. A solution comprising 0.1 M $Zn(CH_3COO)_2.2H_2O$ (zinc acetate dihydrate) was introduced to a solution of 1 M NaOH (sodium hydroxide) in distilled water, and the mixture was heated to 60 °C with continuous stirring using a magnetic stirrer. The resultant white solid products underwent thorough washing with distilled water and ethanol to eliminate residual ions. Subsequently, the purified products were dried at 60 °C in ambient air. Gd-doped ZnO powder samples, with a 3% weight fraction of Gd, were prepared employing the nitric acid method. The synthesis involved nanocrystal zinc oxide, prepared using the sol-gel method, and gadolinium oxide (Gd_2O_3, purity: 99.9%). Controlled amounts of ZnO and Gd_2O_3 powders were meticulously weighed to achieve the desired composition ($Zn_{1-x}Gd_xO$, where x = 0.03). The blending of starting materials occurred at 80 °C in a 1 M nitric acid solution (HNO_3, standard solution) with continuous stirring, conducted in a 250 ml glass beaker. The acid-to-powder ratio was 60 ml per 1 g of initial powders. The mixing process persisted until a dry precursor was obtained, which was then ground in an agate mortar for approximately 15 minutes. Subsequently, the precursor underwent calcination at 300 °C for 5 hours to eliminate potential organic compounds, accompanied by the release of gases such as NO and NO_2. This treatment facilitated the conversion of metallic nitrates to oxides. Finally, the precursor was annealed at 600 °C for 4 hours, leading to the formation of $Zn_{1-x}Gd_xO$ for x = 0.03. Following annealing, the powder samples were cooled to room temperature and triturated in an agate mortar.

The structural characterization of ZnO and ZnO:Gd powder samples was conducted through X-ray powder diffraction (XRD). XRD measurements were acquired within the Bragg

angle 2θ range of ($10^o < 2\theta < 80^o$), employing a Rigaku Miniflex X-ray diffractometer operating at 35 kV, 30 mA, and a scan rate of 0.05 deg.sec^{-1}, with Cu-Kα radiation (λ = 1.5405 Å). Nova NanoSEM 430 scanning electron microscope (SEM) was used to get knowledge about the surface morphology of the nanoparticles. For TL measurements, ZnO and ZnO:Gd powder samples were meticulously deposited onto stainless steel disks using a fine grain technique. The TL glow curves were systematically recorded utilizing a Risø TL/OSL DA-20 reader, incorporating Corning 7/59 and Schott BG/39 optical filters under a nitrogen atmosphere. Throughout the measurement process, a pre-heating protocol was implemented, reaching temperatures up to 140 °C at a heating rate of 2 °C/s, followed by the reading process ascending to 450 °C at a heating rate of 5 °C/s. The TL response to irradiation within the dose range of 30–240 Gy was investigated, utilizing a ^{90}Sr (40 mCi) beta source integrated into the reader setup. This comprehensive approach ensures the elucidation of both structural and dosimetric aspects of the ZnO and ZnO:Gd materials under investigation. The photoluminescence measurements were performed by Perkin Elmer LS55 spectrophotometer at excitation wavelength of 400 nm at room temperature.

3. Results and discussions

Figure 1 presents the XRD patterns for undoped and Gd-doped ZnO within the diffraction angle range of 20-80 degrees. The observed patterns exhibit distinct and intense peaks, closely positioned around the same angles, indicative of the high crystallinity of all synthesized samples. The pronounced sharpness and intensity of these peaks provide robust evidence for the superior crystalline quality of the materials. Upon analyzing the diffraction patterns associated with both undoped and Gd-doped ZnO nanoparticles, the crystal structure was determined to be hexagonal wurtzite, as evidenced by the consistent positions of the peaks [14]. The Miller indices corresponding to the diffraction peaks are conveniently depicted in Figure 1. Remarkably, the XRD patterns of Gd-doped ZnO nanoparticles did not reveal any discernible diffraction peaks related to Gd or Gd_2O_3. This absence strongly suggests that Gd ions have successfully substituted Zn sites within the crystal structure of ZnO during the doping process, confirming the success of the doping procedure. The XRD pattern peaks provide valuable information for determining the average crystallite size (D), a parameter described by the expression

$$D = \frac{K\lambda}{\beta cos\theta} . \quad (1)$$

In this expression, K represents the Scherrer constant, defined as 0.94, and β corresponds to the full-width at half maximum (FWHM) of the observed peak. Utilizing the peak parameters of the three sharpest peaks identified in the XRD pattern and applying them to Eq. (1), the average calculated crystallite sizes for undoped and Gd-doped ZnO nanoparticles were determined to be approximately 21 and 45 nm, respectively. This analysis provides quantitative insights into the crystallite dimensions of the synthesized materials, with the larger size of the Gd-doped ZnO nanoparticles suggesting structural modifications due to the doping process [15,16]. The surface characteristics of the synthesized nanoparticles were analyzed via scanning electron microscopy (SEM) technique. Figure 2 illustrates SEM images depicting the surface morphology of both undoped and Gd-doped ZnO nanoparticles. Inspection of the images reveals that all samples exhibit nanostructured features, with particles predominantly manifesting spherical morphology.

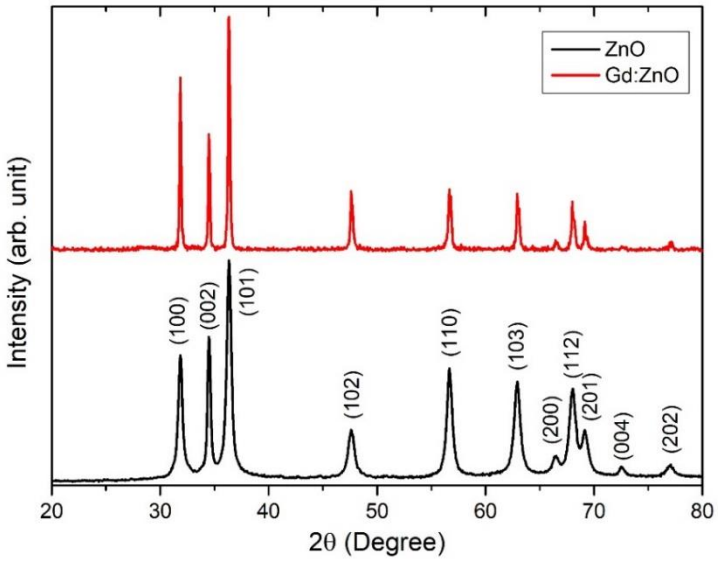

Figure 1. XRD patterns of undoped and Gd-doped ZnO nanoparticles.

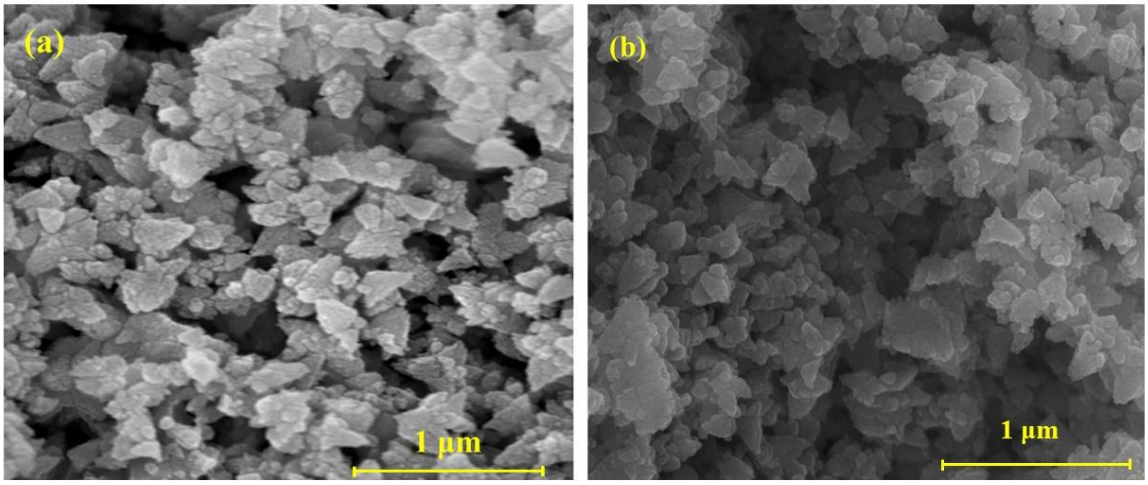

Figure 2. SEM images of the (a) undoped, (b) Gd-doped ZnO nanoparticles.

In order to examine the effect of Gd doping on the TL characteristics of ZnO nanoparticles, TL measurements of undoped and doped nanoparticles were performed at different doses between 0.143 and 240 Gy. However, no peak was observed in the TL curves obtained due to measurements for doses lower than 30 Gy. From the TL curves obtained from controlled increased doses, we saw that the TL curves that could be analyzed exist for doses above 30 Gy. Therefore, TL curves between 30-240 Gy were presented in this study. This shows that undoped and Gd-doped ZnO nanoparticles do not appear suitable for low-dose dosimetry applications. Figure 3 shows the TL curves between 320-600 K where peaks of undoped ZnO nanoparticles are observed. The TL curve revealed the presence of two overlapping peaks around 400 and 480 K. It can be seen from the figure that the intensity of the TL peaks increases as the dose increases.

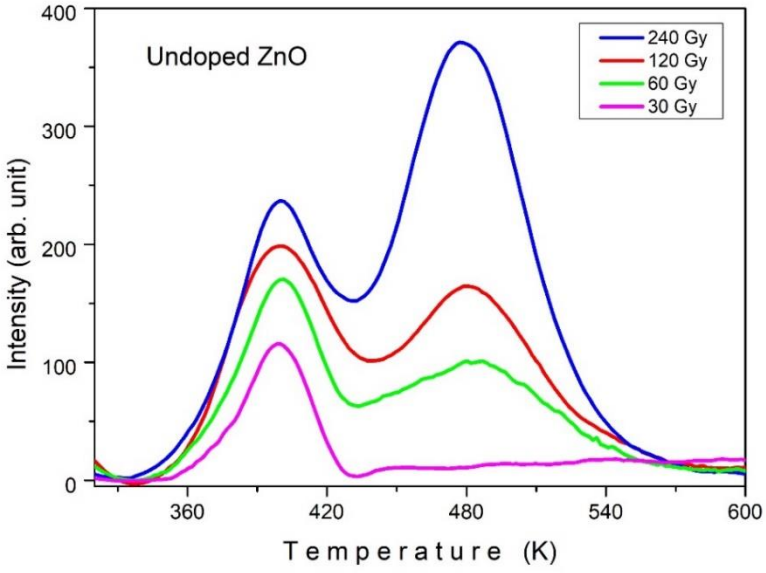

Figure 3. Dose-dependent TL glow curves of undoped ZnO nanoparticles.

Various methodologies are available to ascert the activation energies of trapping centers. In the present investigation, a well-known approach of curve fitting method was applied for the quantitative analysis. The curve fit method, grounded in theoretical principles, involves the fitting of thermoluminescence curves characterized by temperature-dependent functions using specialized software programs. The temperature-dependent TL intensity (I_{TL}) associated with any TL peak is expressed as follows [17]

$$I_{TL} = Cexp\left\{-\frac{E_t}{kT} - \int_{T_0}^{T} \frac{v}{\beta}\exp\left(-\frac{E_t}{kT}\right)dT\right\} \quad \text{(first-order kinetics)} \quad (2)$$

$$I_{TL} = Cexp\left(-\frac{E_t}{kT}\right)\left[1 + (b-1)\frac{n_0 v}{\beta N}\int_{T_0}^{T}\exp\left(-E_t/kT\right)dT\right]^{-\frac{b}{b-1}} \quad \text{(non-first order kinetics)} \quad (3)$$

where C is a constant, n_0 is initial trapped concentration, N is total concentration of the trap centers, v is attempt-to-escape frequency, and b is order of kinetics parameter which takes value $1< b \leq 2$ for non-first order of kinetics. Distinguishing between first and non-first order kinetics is synonymous with characterizing slow and fast retrapping phenomena, respectively. In instances of slow retrapping, the recombination probability of charge carriers, excited to the delocalized bands from trap centers, is notable as opposed to undergoing retrapping. Processes dominating scenarios with slow or negligible retrapping predominantly involve the release of charge carriers from trapping centers and recombining with opposite charge carriers.

Conversely, in cases of fast retrapping, charge carriers are more prone to be retrapped. Applying the curve fitting method to the TL curve consisting of two trapping centers yielded a concordance between theoretical considerations and experimental data, as depicted in Figure 3. The basic calculations and assumptions on which the curve fit application is based are reported in detail in Ref. [18]. The curved fit application was carried out using the OriginPro 9.0 software program. The success of the fitting process is particularly pronounced in situations characterized by non-first order retrapping. This favorable outcome strongly indicates the significance of retrapping for the identified traps within the ZnO nanoparticles underscoring the importance of this research. In Figure 4, the circles correspond to the experimental data, displaying well-fitted two peaks characterized by activation energies of E_{tA} = 0.84 eV and E_{tB} = 1.05 eV. The peak maximum temperatures and order of kinetics extracted from the fitting process for the deconvoluted curves are determined as T_A = 400.5 K, T_B = 479.2 K, b_A = 1.80, and b_B = 1.95. The precision of the decomposition process was evaluated by computing the figure of merit (FOM) for each of the TL glow peaks considering the following expression [19]

$$FOM = \frac{\sum_i |y_{exp} - y_{fit}|}{\sum_i y_{fit}} \quad (4)$$

where y_{exp} and y_{fit} describe the experimental and fitted data, respectively. Based on numerous experiences, it can be concluded that FOM values falling within the range of 0.0% to 2.5% indicate a good fit, while values between 2.5% and 3.5% suggest a minor deviation, and values exceeding 3.5% indicate a poor fit [19]. FOM value was found from Eq. (4) as 2.2%, which points out the fitted curve as a good fit. Many studies are in the literature on the TL properties of doped and undoped ZnO nanoparticles. The TL curve of undoped ZnO nanophosphors showed the presence of two peaks with peak maximum temperatures of 420 and 490 K [20]. The activation energies of these peaks were reported as 0.8 and 1.2 eV, respectively. Applying the curve fitting method to the TL curve of ZnO samples presented three trap centers at 0.58, 0.85, and 1.05 eV [21]. Activation energies of revealed two trap centers in undoped ZnO nanorods were determined as 0.54 and 0.89 eV [22]. Considering the type of ZnO compound studied, the difference in the experimental parameters applied, and the differences in the analysis methods used to obtain the activation energy, it can be said that the energies found as 0.8 and 1.2 eV in this study are compatible with the previously reported values.

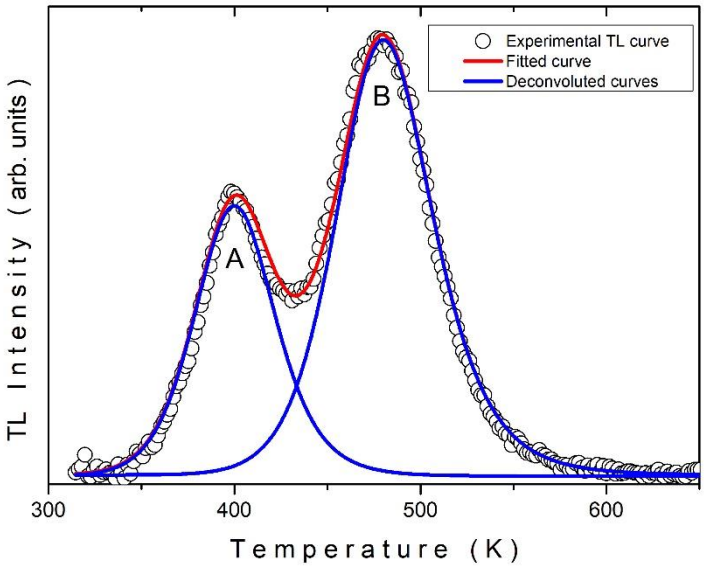

Figure 4. Deconvolution of TL glow curve of ZnO nanoparticles.

To examine the effect of Gd doping on the TL properties of ZnO nanoparticles, the measurements and analysis mentioned above were also performed on Gd-doped ZnO nanoparticles. Figure 5 shows the dose-dependent TL curves of ZnO nanoparticles doped with 3% Gd. While the peak maximum point is observed around 460 K in the TL curve, it is seen that there is a bulge of around 527 K in the region where the peak is decreasing. This indicates that the observed peak consists of overlapped peaks. The part where the TL curves descend after the peak maximum point theoretically shows sharper decreasing behavior in the first-order kinetics, while in the second-order kinetics, the TL curve emerges symmetrically. Considering this situation, the TL curve was expected to decrease to zero around 600 K. However, in the observed TL curve, the peak has an intensity between 600-700 K that cannot be associated with the background. This can only be explained by the presence of a discrete peak in this region. The curve fitting method was also successfully applied to the TL curve of Gd-ZnO nanoparticles. Figure 6 shows the fitted curve and three discrete peaks obtained due to the curve fit method applied to the experimental TL curve. When the TL curves of undoped and Gd-doped ZnO nanoparticles are compared, it is seen that the peak observed around 480 K appears in both materials. In the TL curve of Gd-doped ZnO nanoparticles, two peaks were not observed in the TL curve of undoped ZnO nanoparticles. Since the peak of around 480 K is common for both materials, the peaks observed in Gd-doped ZnO nanoparticles are named as B, C, and D (see Figure 6). The energies of the trap centers revealed from the curve fit method were found

to be E_{tB} = 1.10 eV, E_{tC} = 1.18 eV and E_{tD} = 1.25 eV. The peak maximum temperatures were found as T_B = 482.0 K, T_C = 544.1 K, and T_D = 655.3 K, and order of kinetics were obtained as b_B = 1.80, b_C = 1.96 and b_B = 1.90. FOM value was found for the analysis of Gd-doped ZnO as 1.9% which indicates the fitted curve as good fit.

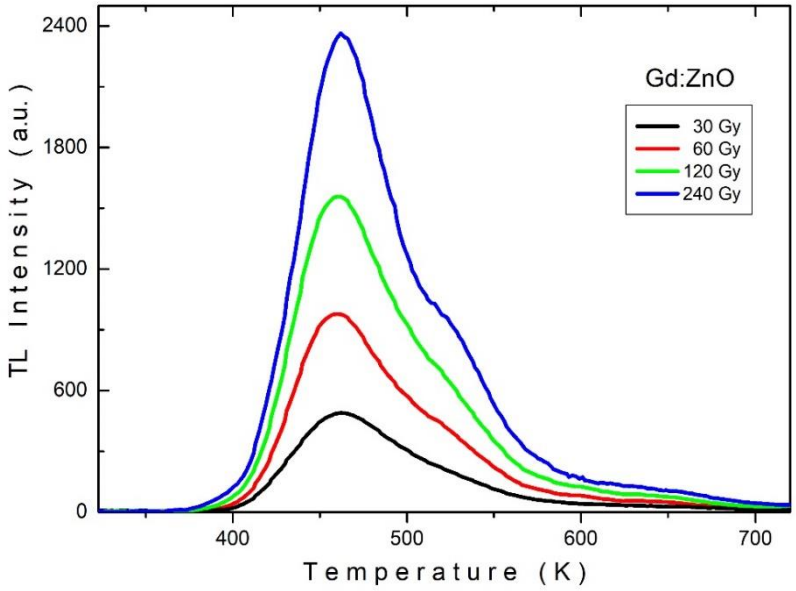

Figure 5. Dose-dependent TL glow curves of Gd-doped ZnO nanoparticles.

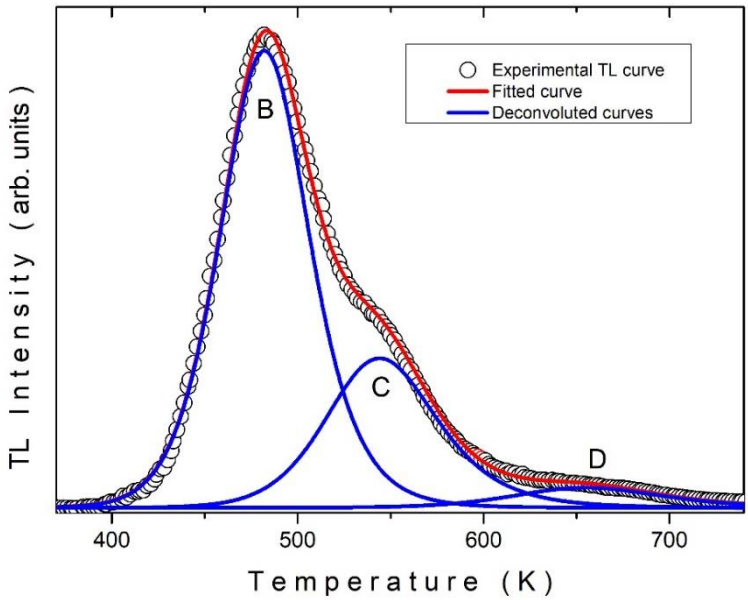

Figure 6. Deconvolution of TL glow curve of Gd-doped ZnO nanoparticles.

A well-known analysis method used to find the activation energies of the first appearing peak in TL glow curves is the initial rise method. This method is centered on the recognition that the integrals in the equations for both first and non-first order reactions (Eqs. 2 and 3) decrease notably as charge carriers commence transitioning from trap levels. Thus, the exponential components within these integrals approximately equal unity within this initial temperature range. Consequently, the thermoluminescence intensity is expressed as follows:

$$I_{\mathrm{TL}} = Cexp(-E_t/kT). \tag{5}$$

According to this equation, the plot of ln(I_{TL}) against 1/T plot shows a linear trend in the initial segment, corresponding to the onset of the TL peak, enabling the determination of activation energy. In this approach, when analyzing graphs with overlapping peaks, only the activation energy of the initial peak is extracted. Thus, we employed the initial rise method to ascertain the activation energies of peak A for undoped ZnO and peak B for Gd-doped ZnO nanoparticles. Figure 7 illustrates the ln(I_{TL}) vs. 1/T plots derived from the above-presented corresponding TL curves (Figures 4 and 6). Through linear regression fitting, activation energies for peak A and B were determined as E_{tA} = 0.86 eV and E_{tC} = 1.05 eV, respectively. These values are compatible with the results found from the curve fit method, and this compatibility may be evidence that the curve fit method is implemented in a reasonable way.

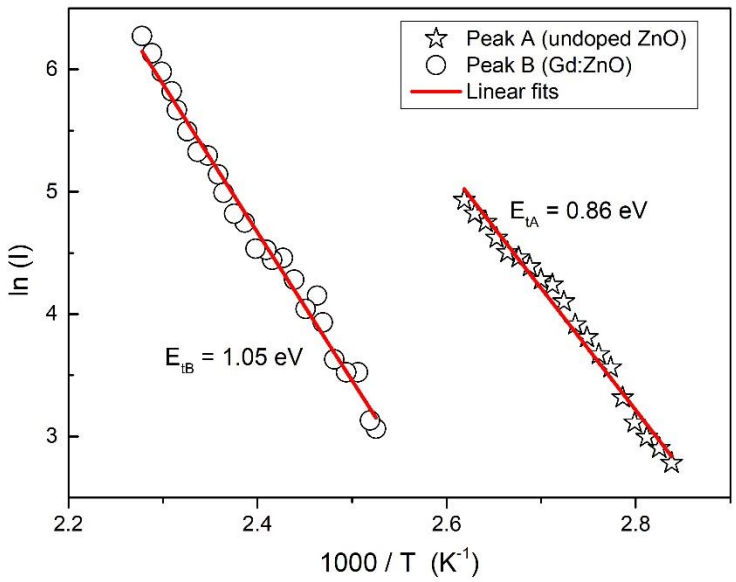

Figure 7. Initial rise method analysis for first appearing peaks in TL curves of undoped and Gd-doped ZnO nanoparticles.

The kinetic parameters found as a result of the curve fit method can be used to find the frequency factor (ν) of the trap centers. The frequency factor and other kinetic parameters (β, T_m, E_t) are formulated as follows [23,24]:

$$\frac{\beta E_t}{kT_m^2} = \nu \exp(-E_t/kT_m)\,[1 + (b-1)\Delta_m] \quad (6)$$

where $\Delta_m = 2kT_m/E_t$. The frequency factors calculated using Eq. (6) are given in Table 1.

Table 1. Kinetic parameters of undoped and Gd-doped ZnO nanoparticles.

Compound	Peak	T_m (K)	E_t (eV)	b	ν (s^{-1})
ZnO	A	400.5	0.84	1.80	1.27×10^{10}
	B	479.2	1.05	1.95	3.32×10^{10}
Gd:ZnO	B	482	1.10	1.80	9.77×10^{10}
	C	544.1	1.18	1.96	2.23×10^{10}
	D	655.3	1.25	1.90	7.86×10^{8}

Dose-dependent graphs of the area under the TL curves of undoped and Gd-doped ZnO nanoparticles are shown in Figure 8. As can be seen from the figure, dose-area dependence exhibited a linear behavior in the studied dose range. The linear behavior of the dose-dependent area graph is a desirable characteristic in dosimetric materials for radiation dosimetry applications, as it simplifies the calibration process. Both studied nanoparticles show significant promise as a dosimeter for monitoring ionizing radiation in various fields. Linear behavior has also been observed before in similar studies on ZnO. As a result of TL measurements in the 10-150 Gy dose range on ZnO phosphors, a linear dose-TL area dependence was reported [21]. TL properties of undoped and Yb-doped ZnO nanophosphors were investigated, and TL behavior of both samples exhibited a linear dose-Tl area dependence [20]. Ag-doped ZnO thin films were studied to get their potential for radiation technology using thermoluminescence measurements [25]. The linear-dependent behavior of the TL signal to the dose, dosimeter sensitivity, thermal and optical fading properties of the films indicated that Ag-doped ZnO thin films exhibit suitable TL characteristics for radiation monitoring.

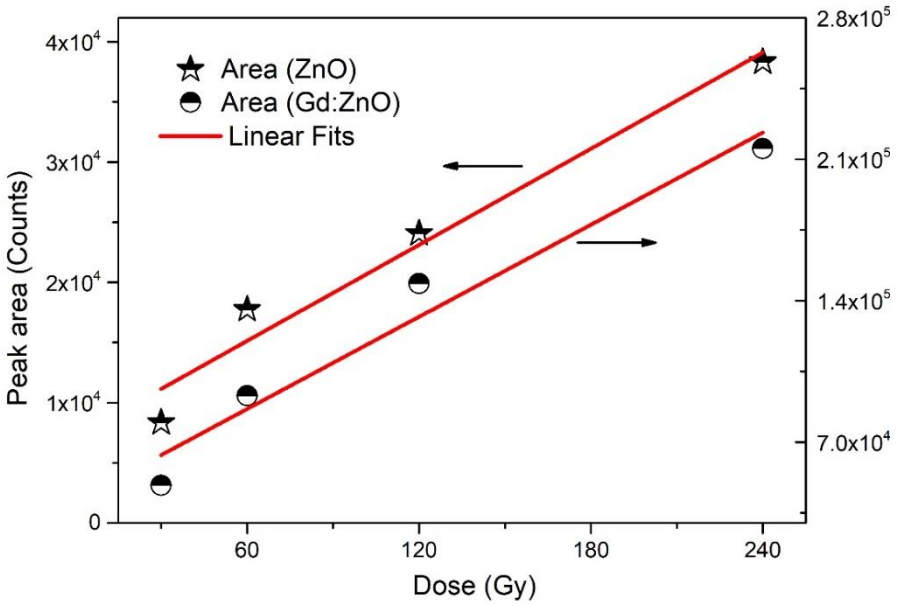

Figure 8. Dose-dependencies of TL peak area of undoped and Gd-doped ZnO nanoparticles. Solid lines represent the applied linear fits.

Figure 9 shows PL spectra of undoped and Gd-doped ZnO nanoparticles with an excitation wavelength of 400 nm. Two peaks around 455 and 577 nm were observed in each spectrum. The peak intensity observed around 455 nm was recorded as almost the same for both nanoparticles. However, the intensity of the observed peak was around 577 nm, which was observed to be higher for the Gd-doped nanoparticle. ZnO compound exhibits various emission peaks between 400 and 600 nm. The emission peaks were associated with native defects like oxygen vacancy (V_o), zinc vacancy (V_{zn}), zinc interstitial (Zn_i) and oxygen antisities (O_{zn}) [26–28]. The blue emission peak around 455 nm was previously observed in many studies. In Ref. [29], PL spectrum of the ZnO thin films presented peak around 456 nm. The authors stated that the observed emission likely arises from an electronic transition between the donor level of Zn interstitial and the acceptor energy level of Zn vacancy. In Ref. [30], a blue emission peak was observed around 449 nm in the PL spectrum of ZnO nanoparticles. Authors attributed this peak to Zn_i along with OH^- ions present at the surface of nanoparticles. The green emission in the ZnO compound was reported in many studies before. In related studies, green emission peak in the PL spectrum was recorded at different wavelengths like 510 nm [26], 557 nm [30], 580 nm [31] and 550 nm [32]. The presence of deep-level oxygen vacancies creates localized states within the bandgap of the material. Electrons can get trapped in these vacancies, and when they

recombine with holes (positively charged carriers), light emission occurs. The peak observed in the green region of the spectrum was associated with this recombination process.

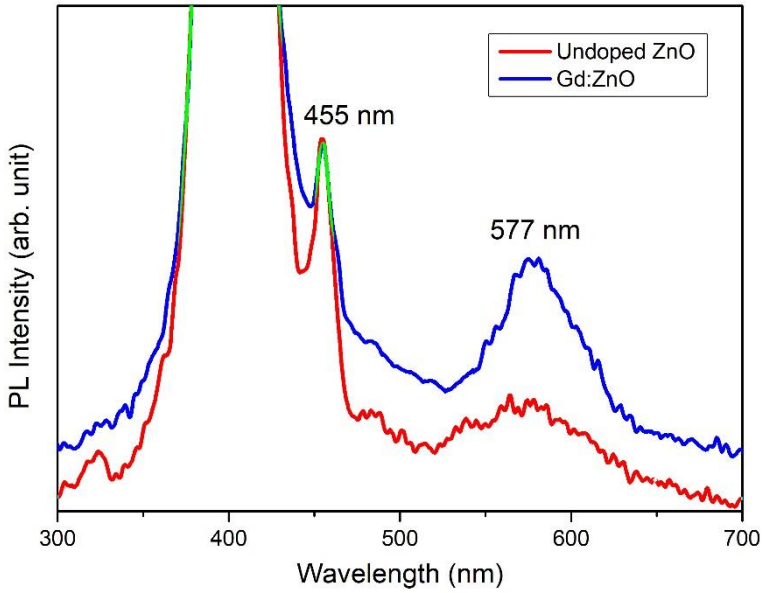

Figure 9. PL spectrum of undoped and Gd-doped ZnO nanoparticles.

4. Conclusion

In conclusion, our investigation into the thermoluminescence behavior of undoped and Gd-doped ZnO nanoparticles unravels intricate details governing their trap centers and activation energies. TL glow curves were analyzed using the curve fitting method. Examining the thermoluminescence (TL) curve for undoped ZnO nanoparticles disclosed the existence of two trap centers at energy levels of 0.84 eV and 1.05 eV. In contrast, Gd-doped ZnO nanoparticles exhibited a more complex TL curve, revealing the presence of three distinct trapping centers characterized by energies of 1.10 eV, 1.18 eV, and 1.25 eV. The absence of the 0.84 eV trap center in Gd-doped ZnO suggests a dopant-induced alteration in defect configurations. It is thought that the levels of 1.05 and 1.10 eV revealed for undoped and Gd-doped ZnO nanoparticles belong to the same trap centers. Remarkably, the emergence of new peaks at 1.18 eV and 1.25 eV exclusively in Gd-doped ZnO accentuates the dopant's role in introducing novel trap centers. The observed linear dose-dependent behavior in both types of nanoparticles signifies the dosimetric potential of these nanoparticles. Photoluminescence spectra of undoped and Gd-doped compounds presented a blue emission peak of around 455 and a green emission peak of around 577 nm. These peaks were associated with zinc interstitial and oxygen vacancy native defects in the compound.

Acknowledgments

This work was supported by the Scientific and Technological Research Council of Turkey, 1001 Scientific and Technological Research projects, No:110T345.

References

[1] Sharanu, Kompa A, Pal A and Rao K M 2023 Structural, spectroscopic, and electrical studies of spin-coated ZnO-ZTO thin films for their potential application in photocatalysis and optoelectronics *Ceram Int* **49** 18272–80

[2] Elzawiei Y S M, Abdulhameed A, Hashim M R and Halim M M 2023 A study of the UV photodetectors properties based on the effect of TiO2 on ZnO nanorods grown via the chemical bath deposition method on p-type Si (100) substrates *Opt Mater (Amst)* **144** 114353

[3] Muhammad A, Mohammad S M, Hassan Z, Rajamanickam S, Abed S M and Ashiq M G B 2023 Fabrication of fluorine and silver co-doped ZnO photodetector using modified hydrothermal method *Microelectronics International* **40** 1–7

[4] Zeng J, Qi Y, Liu Y, Chen D, Ye Z and Jin Y 2022 ZnO-Based Electron-Transporting Layers for Perovskite Light-Emitting Diodes: Controlling the Interfacial Reactions *J Phys Chem Lett* **13** 694–703

[5] Zhang Y, Jiang Y, Ma C, Zhang J and Yang B 2023 Preparation of ZnO Piezoelectric Thin-Film Material for Ultrasonic Transducers Applied in Bolt Stress Measurement *Coatings* **13** 1538

[6] Li Z, Li Z, Shi Z, Zhu P, Wang Z, Zhang J, Li Y, He P and Zhang S 2023 ALD prepared silver nanowire/ZnO thin film for ultraviolet detectors *Mater Today Commun* **37** 106974

[7] Essalah G, Guermazi H, Guermazi S, Jedryka J, Ozga K, Antony A, Rao A and Poornesh P 2023 Enhanced sunlight photo-catalytic performances of ZnO/ZnNb2O6/Nb2O5 composites for organic pollutant degradation *Opt Mater (Amst)* **138** 113637

[8] Masuda Y 2023 Cold crystallization and morphology control of ZnO nanostructures for chemical sensors *Int J Appl Ceram Technol* **20** 585–611

[9] Shakoor A, Nowsherwan G A, Alam W, Bhatti S Y, Bilal A, Nadeem M, Zaib A and Hussain S S 2023 Fabrication and characterization of TiO2: ZnO thin films as electron transport material in perovskite solar cell (PSC) *Physica B Condens Matter* **654** 414690

[10] Cruz-Vázquez C, Burruel-Ibarra S E, Grijalva-Monteverde H, Chernov V and Bernal R 2007 Thermally and optically stimulated luminescence of new ZnO nanophosphors exposed to beta particle irradiation *Radiation Effects and Defects in Solids* **162** 737–43

[11] Cruz-Vázquez C, Bernal R, Burruel-Ibarra S E, Grijalva-Monteverde H and Barboza-Flores M 2005 Thermoluminescence properties of new ZnO nanophosphors exposed to beta irradiation *Opt Mater (Amst)* **27** 1235–9

[12] Liuxi Tan, Jia Li, Kai Wang and Sheng Liu 2009 Effects of Defects on the Thermal and Optical Performance of High-Brightness Light-Emitting Diodes *IEEE Transactions on Electronics Packaging Manufacturing* **32** 233–40

[13] Buffolo M, Caria A, Piva F, Roccato N, Casu C, De Santi C, Trivellin N, Meneghesso G, Zanoni E and Meneghini M 2022 Defects and Reliability of GaN-Based LEDs: Review and Perspectives *physica status solidi (a)* **219**

[14] Isik M and Gasanly N M 2019 Gd-doped ZnO nanoparticles: Synthesis, structural and thermoluminescence properties *J Lumin* **207** 220–5

[15] Hannachi E, Slimani Y, Nawaz M, Sivakumar R, Trabelsi Z, Vignesh R, Akhtar S, Almessiere M A, Baykal A and Yasin G 2023 Preparation of cerium and yttrium doped ZnO nanoparticles and tracking their structural, optical, and photocatalytic performances *Journal of Rare Earths* **41** 682–8

[16] Althobaiti M G, Alotaibi A A, Alharthi S S and Badawi A 2022 Modification of the structural, linear and nonlinear optical properties of zinc oxide thin films via barium and magnesium doping *Opt Mater (Amst)* **131** 112646

[17] Chen R, Lawless J L and Pagonis V 2022 On the various-heating-rates method for evaluating the activation energies of thermoluminescence peaks *Radiat Meas* **150** 106692

[18] Isik M, Goksen K, Gasanly N M and Ozkan H 2008 Trap Distribution in TlInS2 Layered Crystals from Thermally Stimulated Current Measurements *Journal of the Korean Physical Society* **52** 367–73

[19] Balian H G and Eddy N W 1977 Figure-of-merit (FOM), an improved criterion over the normalized chi-squared test for assessing goodness-of-fit of gamma-ray spectral peaks *Nuclear Instruments and Methods* **145** 389–95

[20] Pal U, Meléndrez R, Chernov V and Barboza-Flores M 2006 Thermoluminescence properties of ZnO and ZnO:Yb nanophosphors *Appl Phys Lett* **89**

[21] Borbón-Nuñez H A, Iriqui-Razcón J L, Cruz-Vázquez C, Bernal R, Furetta C, Chernov V and Castaño V M 2017 Thermoluminescence kinetics parameters of ZnO exposed to beta particle irradiation *J Mater Sci* **52** 5208–15

[22] Pal P P and Manam J 2013 Photoluminescence and thermoluminescence studies of Tb3+ doped ZnO nanorods *Materials Science and Engineering: B* **178** 400–8

[23] Pushpa N, Kokila M K and Nagabhushana K R 2016 Thermoluminescence studies of γ-irradiated ZnO:Mg2+ nanoparticles *Nucl Instrum Methods Phys Res B* **379** 62–8

[24] Kitis G, Gomez-Ros J M and Tuyn J W N 1998 Thermoluminescence glow-curve deconvolution functions for first, second and general orders of kinetics *J Phys D Appl Phys* **31** 2636–41

[25] Thabit H A, Kabir N A, Ismail A K, Alraddadi S, Bafaqeer A and Saleh M A 2022 Development of Ag-Doped ZnO Thin Films and Thermoluminescence (TLD) Characteristics for Radiation Technology *Nanomaterials* **12** 3068

[26] Djurišić A B, Leung Y H, Tam K H, Hsu Y F, Ding L, Ge W K, Zhong Y C, Wong K S, Chan W K, Tam H L, Cheah K W, Kwok W M and Phillips D L 2007 Defect emissions in ZnO nanostructures *Nanotechnology* **18** 095702

[27] Ton-That C, Weston L and Phillips M R 2012 Characteristics of point defects in the green luminescence from Zn- and O-rich ZnO *Phys Rev B* **86** 115205

[28] McCluskey M D and Jokela S J 2009 Defects in ZnO *J Appl Phys* **106**

[29] Wei X, Zhao R, Shao M, Xu X and Huang J 2013 Fabrication and properties of ZnO/GaN heterostructure nanocolumnar thin film on Si (111) substrate *Nanoscale Res Lett* **8** 112

[30] Jayachandraiah C and Krishnaiah G 2017 Influence of cerium dopant on magnetic and dielectric properties of ZnO nanoparticles *J Mater Sci* **52** 7058–66

[31] Aravapalli Vanaja, Suresh M, Jeevanandam J, Venkatesh, Gousia Sk, Pavan D, Balaji D and Murthy N B 2019 Copper-Doped Zinc Oxide Nanoparticles for the Fabrication of white LEDs *Protection of Metals and Physical Chemistry of Surfaces* **55** 481–6

[32] Saikia L, Bhuyan D, Saikia M, Malakar B, Dutta D K and Sengupta P 2015 Photocatalytic performance of ZnO nanomaterials for self sensitized degradation of malachite green dye under solar light *Appl Catal A Gen* **490** 42–9